Proceedings of the WORKSHOP on
Fundamental Issues and Future Research Directions for Parallel Mechanisms and Manipulators
October 3–4, 2002, Quebec City, Quebec, Canada
Clément M. Gosselin and Imme Ebert-Uphoff, editors

Architecture Independent Workspace Analysis of Planar Three-Legged Manipulators

M.J.D. HAYES
Mechanical & Aerospace Engineering
Carleton University
1125 Colonel By Drive
Ottawa, ON, Canada, K1S 5B6
jhayes@mae.carleton.ca

Abstract: *A method for determining the reachable workspace of general planar three degree of freedom platforms with three legs of arbitrary architecture is presented, where only the active joints are in the presence of limits. A brief review of kinematic mapping is given. The kinematic image of the workspace consists of solid regions bounded by the intersection of minimum and maximum joint input constraint surfaces, a pair for each platform leg. The condition that the leg joining the moving platform to the fixed base be connected with three independent one degree of freedom lower pair joints is employed. Because the procedure uses position-level constraint surfaces in a kinematic image space, it additionally allows for the analysis of some platforms containing holonomic higher pairs.*

1 Introduction

Research interest in parallel manipulators has grown steadily over the last twenty-five years. This is partly due to their inherent advantages over serial manipulators where accuracy, stiffness, load-to-weight-ratio and operating speeds are concerned [1]. One major disadvantage of parallel manipulators in general, compared to serial ones, is that their reachable workspace is small and may contain a high density of interior singularities [2, 3]. Although the workspace analysis of planar three-legged manipulators is well established, see [4, 5, 6] for example, there exists no unified approach that is architecture independent. This gives the motivation for the work presented herein.

In this paper kinematic mapping is used to analyze the reachable workspace planar three-legged platforms of arbitrary architecture in the presence of joints limits on only the actuated joints. Such a *general planar three-legged platform* (GP3LP) consists of a moving platform connected to a fixed base by three kinematic chains. Each chain is connected by three independent one degree-of-freedom (DOF) joints, one of which is active, see [7, 8]. The method employed is based on that found in [6], wherein platforms consisting of three revolute-prismatic-revolute (RPR) legs, the actuated joint being the P-pair, are analyzed. This approach can be generalized to all possible GP3LP due to the results presented in [9] and [10]. It can also be adapted for analysis of a sub-class of platforms with actuated holonomic higher pairs [11].

For GP3LP with three DOF we consider the motions of the platform by examining the motions of each leg separately. The kinematic mapping transforms distinct planar displacements of a reference frame rigidly attached to the platform to distinct points in a three dimensional projective image space. When the joints are restricted to lower-pairs, *prismatic* (P) and *revolute* (R) pairs, then depending on the details of how the kinematic chain is arranged the image space point sets can be one of only two types: 1) if the constraint is linear (a point on the moving platform remains on a fixed line, or the inversion of a line on the platform moving on a fixed point) the corresponding image space point set is an hyperbolic paraboloid; 2) if the constraint is circular (a point on the moving platform remains on a fixed circle) the corresponding image space point set is an hyperboloid of one sheet [9]. Because these quadric surfaces contain the images of the constrained displacements, it is natural to call them *constraint surfaces*. Kinematic analysis of GP3LP reduces to intersection problems between the constraint surfaces for each leg.

Because of the illustrative description of all possible positions of the end-effector system as a surface-bound solid region in an image space, it is believed that this is a useful tool for designers. Moreover, it facilitates computations when the reachable workspace of more than one reference point in the end-effector system has to be determined.

2 Classifying General Planar Three-Legged Platforms

A GP3LP with three DOF consists of a moving platform connected to a fixed base by three simple kinematic chains. Each

chain is connected by three independent one DOF joints, one of which is active. Thus each chain provides the control of one of three DOF of the moving platform. Since the displacements of the platform are confined to the plane, only R- and P-pairs are used. But, in certain cases a holonomic higher gear pair (G) can replace a lower R-, or P-pair (one such platform is considered in Section 5.3. Platform motions are characterized by the motion of reference frame E, attached to the moving platform, relative to frame Σ, attached to the non-moving base, see Figure 1.

The possible combinations of R- and P-pairs which connect the moving platform to the fixed base and constrain the independent open kinematic chains, consisting of successions of three joints starting from the fixed base, in a GP3LP are [7]:

$$RRR,\ RPR,\ RRP,\ RPP,\ PRR,\ PPR,\ PRP,\ PPP.$$

We must, however, exclude the PPP chain because no combination of pure planar translations can cause a change in orientation. Thus, there are seven possible kinematic chains, which may be combined in either topologically symmetric or asymmetric groups of three. Figure 2 illustrates topologically symmetric platforms, each characterized by one of the seven allowable simple kinematic chains. For our working definitions of topological symmetry and asymmetry, see the last paragraph in Section 2.1.

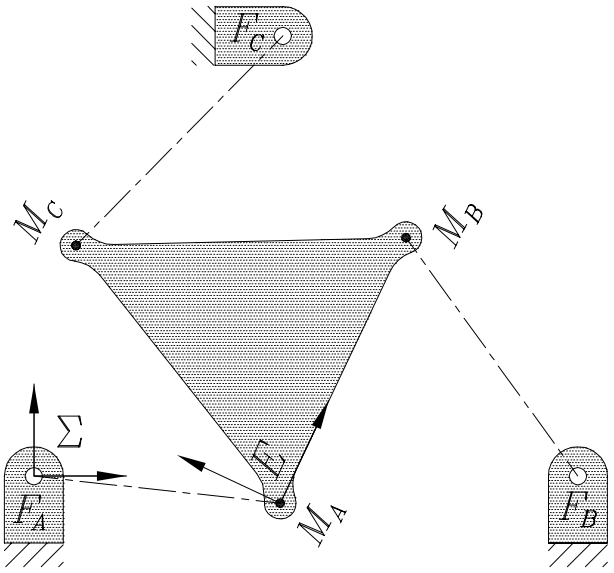

Figure 1: The moving frame E and fixed frame Σ for any combination of legs from Table 1.

2.1 Passive Sub-chains

The active joint in a leg is identified with an underscore, $R\underline{P}R$, for example. Since any one of the three joints in any of the seven allowable simple kinematic chains may be actuated there are twenty-one possible leg architectures.

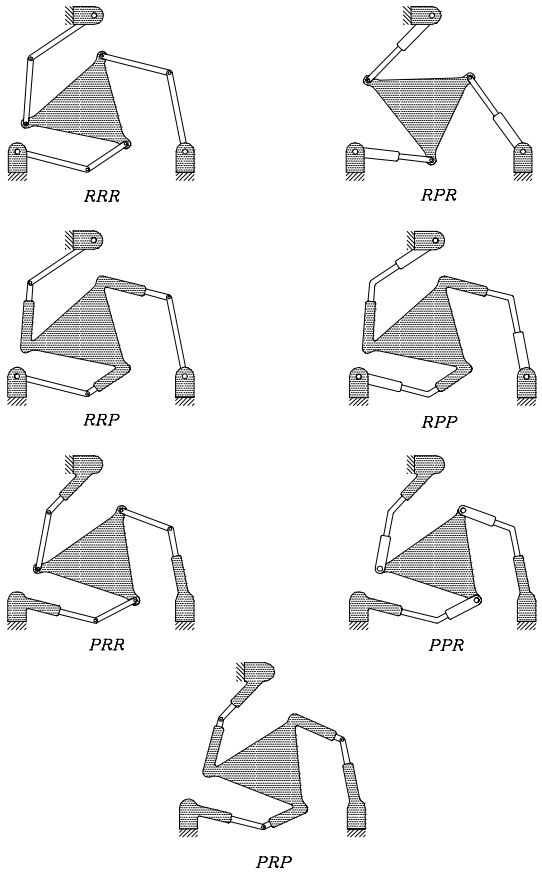

Figure 2: The seven possible leg topologies in *symmetric* platforms. When the legs are not all the same, the platform is *asymmetric*.

When the value of the activated joint coordinate in a leg is specified, the joint is effectively locked and may be temporarily removed from the chain. What remains is a kinematic chain connected with two passive joints. Examining Figure 2, it is to be seen that the resulting passive sub-chain is one of only four types: either RR, PR, RP, or PP. For now we exclude PP-type legs from the enumeration since platforms containing two or three such legs either move uncontrollably or are not assemblable when the actuated joint variables are specified [7, 12]. Nonetheless, platforms containing one PP-type leg are feasible. They are discussed in Section 4.4, but are not included in the enumeration because the expression of their constraints in a way that is compatible with the kinematic mapping remains an open, but likely straightforward, problem. This reduces the number of possible leg architectures to eighteen. They are listed, according to passive sub-chain, in Table 1.

The platform is considered to be *symmetric* when all three legs are the same type, each possessing the same type of actuated joint at the same location in the kinematic chain. The leg is otherwise considered to be *asymmetric*.

RR-type	PR-type	RP-type
$\underline{R}RR$	$\underline{R}PR$	$\underline{R}RP$
$R\underline{R}R$	$P\underline{R}R$	$R\underline{R}P$
$RR\underline{R}$	$PR\underline{R}$	$RP\underline{R}$
$\underline{P}RR$	$\underline{P}PR$	$\underline{P}RP$
$R\underline{P}R$	$P\underline{P}R$	$R\underline{P}P$
$RR\underline{P}$	$PR\underline{P}$	$RP\underline{P}$

Table 1: The 18 possible leg architectures.

2.2 Enumerating the GP3LP

How many distinct GP3LP with three DOF are there? This number is arrived at by considering that there are 18 possible kinematic chains to choose from for each leg. A selection of r different elements taken from a set of n, without regard to order, is a combination of the n elements taken r at a time. If the elements are allowed to be counted more than once the number of possible combinations is given by

$$\begin{aligned} C(n,r) &= \frac{(n+r-1)!}{r!(n-1)!} \\ \Rightarrow C(18,3) &= 1140. \end{aligned} \tag{1}$$

3 Planar Mapping

Consider the reference frame E which can undergo general planar displacements relative to reference frame Σ, as illustrated in Figure 1. Let the homogeneous coordinates of points in the moving frame E be the ratios $(x : y : z)$, and homogeneous coordinates of the same point, but expressed in the fixed frame Σ, be the ratios $(X : Y : Z)$. The homogeneous transformation that maps points in E to Σ can be written as

$$\begin{bmatrix} X \\ Y \\ Z \end{bmatrix} = \begin{bmatrix} \cos\varphi & -\sin\varphi & a \\ \sin\varphi & \cos\varphi & b \\ 0 & 0 & 1 \end{bmatrix} \begin{bmatrix} x \\ y \\ z \end{bmatrix}. \tag{2}$$

Equation (2) underscores the fact that a general planar displacement is characterized by the three parameters a, b, and φ, where a and b are the (X, Y) coordinates of the origin of E expressed in Σ and φ is the orientation of E relative to Σ, respectively.

The essential idea of the kinematic mapping, introduced simultaneously but independently by Blashke [13] and Grünwald [14] in 1911, is to map the three homogeneous coordinates of the pole of a planar displacement, in terms of (a, b, φ), to the points of a three dimensional projective image space. The kinematic mapping image coordinates are defined as:

$$\begin{aligned} X_1 &= a\sin(\varphi/2) - b\cos(\varphi/2) \\ X_2 &= a\cos(\varphi/2) + b\sin(\varphi/2) \\ X_3 &= 2\sin(\varphi/2) \\ X_4 &= 2\cos(\varphi/2). \end{aligned} \tag{3}$$

Since each distinct displacement described by (a, b, ϕ) has a corresponding unique image point, the inverse mapping can be obtained from Equation (3): for a given point of the image space, the displacement parameters are

$$\begin{aligned} \tan(\varphi/2) &= X_3/X_4, \\ a &= 2(X_1X_3 + X_2X_4)/(X_3^2 + X_4^2), \\ b &= 2(X_2X_3 - X_1X_4)/(X_3^2 + X_4^2). \end{aligned} \tag{4}$$

Equations (4) give correct results when either X_3 or X_4 is zero. Caution is in order, however, because the mapping is injective, not bijective: *there is at most one pre-image for each image point*. Thus, not every point in the image space represents a displacement. It is easy to see that any image point on the real line $X_3 = X_4 = 0$ has no pre-image and therefore does not correspond to a real displacement of EE. From Equation (4), this condition renders φ indeterminate and places a and b on the line at infinity.

By virtue of the relationships expressed in Equation (3), the transformation matrix from Equation (2) may be expressed in terms of the homogeneous coordinates of the image space. This yields a linear transformation to express a displacement of E with respect to Σ in terms of the image point [15]:

$$\begin{bmatrix} X \\ Y \\ Z \end{bmatrix} = \boldsymbol{T} \begin{bmatrix} x \\ y \\ z \end{bmatrix}, \tag{5}$$

where

$$\boldsymbol{T} = \begin{bmatrix} X_4^2 - X_3^2 & -2X_3X_4 & 2(X_1X_3 + X_2X_4) \\ 2X_3X_4 & X_4^2 - X_3^2 & 2(X_2X_3 - X_1X_4) \\ 0 & 0 & X_3^2 + X_4^2 \end{bmatrix}.$$

The inverse transformation can be obtained with the inverse of the matrix in Eq. (5) as follows.

$$\begin{bmatrix} x \\ y \\ z \end{bmatrix} = \boldsymbol{T}^{-1} \begin{bmatrix} X \\ Y \\ Z \end{bmatrix}, \tag{6}$$

with

$$\boldsymbol{T}^{-1} = \begin{bmatrix} X_4^2 - X_3^2 & 2X_3X_4 & 2(X_1X_3 - X_2X_4) \\ -2X_3X_4 & X_4^2 - X_3^2 & 2(X_2X_3 + X_1X_4) \\ 0 & 0 & X_3^2 + X_4^2 \end{bmatrix}.$$

Thus, the coordinates of a point $(x, : y : z)$ in the (relatively) moving frame has coordinates $(X, : Y : Z)$ in the (relatively) fixed frame:

$$
\begin{aligned}
X &= (X_4^2 - X_3^2)x - (2X_3X_4)y + 2(X_1X_3 + X_2X_4)z, \\
Y &= (2X_3X_4)x + (X_4^2 - X_3^2)y + 2(X_2X_3 - X_1X_4)z, \\
Z &= (X_3^2 + X_4^2)z. \qquad (7)
\end{aligned}
$$

While the inverse, coordinates of a point $(X, : Y : Z)$ in the (relatively) moving frame has coordinates $(x, : y : z)$ in the (relatively) fixed frame are given by:

$$
\begin{aligned}
x &= (X_4^2 - X_3^2)X + (2X_3X_4)Y + 2(X_1X_3 - X_2X_4)Z, \\
y &= -(2X_3X_4)X + (X_4^2 - X_3^2)Y + 2(X_2X_3 + X_1X_4)Z, \\
z &= (X_3^2 + X_4^2)Z. \qquad (8)
\end{aligned}
$$

4 Constraint Surfaces

The lower-pair constraints on the motion of any particular leg in an arbitrary GP3LP involve only one of the following.

1. A point with fixed coordinates in the moving frame moves on a fixed circle of fixed radius in the fixed frame (*RR*-type constraint).
2. A point with fixed coordinates in the moving frame moves on a fixed line in the fixed frame (*PR*-type constraint).
3. A line with fixed coordinates in the moving frame moves on a fixed point in the fixed frame (*RP*-type constraint).

The last two constraints are kinematically equivalent when considered inversions of each other. It may additionally be argued that the circular constraint is the most general, since a line can always be considered as a circle of infinite radius.

4.1 Implicit Equation of General Constraint Surface

A clearer picture of the image space constraint surface that corresponds to the kinematic constraints emerges when $(X : Y : Z)$, or $(x : y : z)$ from Equations (7), or (8) are substituted into the general equation of a circle, the form of the most general constraint:

$$
K_0(X^2 + Y^2) + 2K_1XZ + 2K_2YZ + K_3Z^2 = 0, \quad (9)
$$

where $[K_0 : K_1 : K_2 : K_3]$ are the *circle coordinates*, with $K_1 = -X_c$, $K_2 = -Y_c$, $K_3 = X_c^2 + Y_c^2 - r^2$, with X_c and Y_c being the coordinates of the circle centre of radius r, and K_0 is an arbitrary homogenising constant. One obtains the following implicit equation of a constraint surface in the image space:

$$
\begin{aligned}
&K_0z^2(X_1^2 + X_2^2) + (-K_0x + K_1z)zX_1X_3 \\
&+(-K_0y + K_2z)zX_2X_3 \mp (K_0y + K_2z)zX_1X_4 \\
&\pm(K_0x + K_1z)zX_2X_4 \mp (K_1y - K_2x)zX_3X_4 \\
&+\frac{1}{4}[K_0(x^2 + y^2) - 2z(K_1x + K_2y) + K_3z^2]X_3^2 \\
&+\frac{1}{4}[K_0(x^2 + y^2) + 2z(K_1x + K_2y) + K_3z^2]X_4^2 = 0. \quad (10)
\end{aligned}
$$

If the kinematic constraint is a fixed point in E bound to a circle ($K_0 = 1$), or line ($K_0 = 0$) in Σ, then $(x : y : z)$ are the coordinates of the platform reference point in E and the upper signs apply. On the other hand, if the kinematic constraint is a fixed point in Σ bound to a circle ($K_0 = 1$), or line ($K_0 = 0$) in E, then $(X : Y : Z)$ are substituted for $(x : y : z)$, and the lower signs apply.

The K_i are functions of the variable joint input parameter. The constraint surfaces defined by the joint input are not arranged arbitrarily in the image space. It turns out that the image of the workspace for a particular leg is bounded by the two constraint surfaces corresponding to the minimum and maximum variable joint input parameters. Moreover, it can be shown that the hyperboloid of one sheet and the hyperbolic paraboloid are the only possible constraint surfaces for such planar three-legged platforms [9].

4.2 Circle Constraints

When one sets $K_0 = 1$, together with $X_4 = z = 1$ in Eq. (10) the result is the implicit equation of a hyperboloid of one sheet in terms of the image space coordinates (X_1, X_2, X_3)[9, 10]:

$$
\begin{aligned}
&(X_1^2 + X_2^2) + (K_1 - x)X_1X_3 + (K_2 - y)X_2X_3 \\
&\mp(K_2 + y)X_1 \pm (K_1 + x)X_2 \pm (K_2x - K_1y)X_3 \\
&+\frac{1}{4}[(x^2 + y^2) - 2(K_1x + K_2y) + K_3]X_3^2 \\
&+\frac{1}{4}[(x^2 + y^2) + 2(K_1x + K_2y) + K_3] = 0. \qquad (11)
\end{aligned}
$$

This hyperboloid has the property that planes parallel to $X_3 = 0$ intersect it in circles, though its axis is not necessarily perpendicular to $X_3 = 0$. For planar three-legged platforms, the inversion of a fixed circle in the moving frame moving on a fixed point in the fixed frame never arises.

All points on this constraint hyperboloid represent displacements of the platform for the given input in the given leg when the remaining two legs have been disconnected from the platform. It can be easily parameterized [9], an example illustrated in Figure 3 shows the minimum and maximum constraint hyperboloids for the three legs of a symmetric $R\underline{P}R$ platform, similar to the one shown in Figure 9.

4.3 Line Constraints

If $K_0 = 0$ in Eq. (9) we obtain a line, which is a real degenerate circle, with *line coordinates* determined by the relation $[L_1 : L_2 : L_3] = [2K_1 : 2K_2 : K_3]$. Setting $K_0 = 0$, together with $X_4 = z = 1$ in Eq. (10) one obtains the implicit equation of a hyperbolic paraboloid in the image space [9, 10]:

$$
\begin{aligned}
&K_1X_1X_3 + K_2X_2X_3 \mp K_2X_1 \pm K_1X_2 \pm (K_2x - K_1y)X_3 \\
&-\frac{1}{4}[2K_1x + 2K_2y - K_3]X_3^2 + \frac{1}{4}[2K_1x + 2K_2y + K_3] = 0. \quad (12)
\end{aligned}
$$

The kinematic inversion between PR- and RP-type legs, unlike the RR case, is a concern here. Equation (12) is used to

represent both. For PR-type legs a point with fixed coordinates in the moving frame moves on a fixed line in the fixed frame. In this case the corresponding constraint equation is given by Equation (12) the upper signs are used. However, for RP-type legs, where the constraint is a line with fixed coordinates in the moving frame moving on a fixed point in the fixed frame, the lower signs are used and x, y, or z is substituted whenever X, Y, or Z are encountered. A parameterized example is illustrated in Figure 5, showing the minimum and maximum constraint hyperbolic paraboloids for the three legs of a symmetric $P\underline{P}R$, similar to the one shown in Figure 4.

4.4 PP-Type Legs

The image space constraint surface corresponding to possible displacements of a PP-type leg is a degenerate quadric that splits into a real and an imaginary plane. This is because only curvilinear motion of the platform can result when the other two platform attachment joints are disconnected: once the angular input of the active R-pair is fixed no rotation of leg or platform is possible. Still, the image of a two parameter family of displacements must be a two parameter constraint manifold, but because φ is constant, the image space coordinates $X_3 = f(\varphi)$ and $X_4 = g(\varphi)$ must also be constant. Hence, the finite part of the two dimensional constraint manifold is linear and must be a hyper-plane.

Moreover, all planes corresponding to possible displacements of the PP-type leg are parallel to $X_3 = 0$. If the platform consists of two, or three PP-type legs, the constraint planes may be distinct, but parallel thereby having no finite points in common; or the planes will be coincident, indicating infinite assembly modes yielding uncontrollable self motions.

There is no practical design merit associated with platforms containing two, or three PP-type legs. This, however, does not preclude designs of topologically asymmetrical three legged planar platforms with at most one PP-type leg. On the other hand, the self-motion property provides possibilities to design very stiff one DOF planar platforms which are relatively easy to actuate.

5 Examples

5.1 Workspace of *R$\underline{P}$R*-Symmetric Platforms

The first use of kinematic mapping for workspace analysis of planar three-legged platforms was in [6]. However, the particular approach is suitable only for $R\underline{P}R$-symmetric platforms, similar to that found in Figure 9.

The first step is to parameterize Equation (11). One possibility is [9]

$$\begin{bmatrix} X_1 \\ X_2 \\ X_3 \end{bmatrix} = \frac{1}{2} \begin{bmatrix} [(\mathcal{K}_1 + x)t - \mathcal{K}_2 + y] + (r_i\sqrt{t^2+1})\cos\zeta \\ [(\mathcal{K}_2 + y)t + \mathcal{K}_1 - x] + (r_i\sqrt{t^2+1})\sin\zeta \\ 2t \end{bmatrix},$$

$$\begin{array}{l} \zeta \in \{0, \ldots, 2\pi\}, \\ t \in \{-\infty, \ldots, \infty\}, \\ i_{min} \le i \le i_{max}, \end{array} \qquad (13)$$

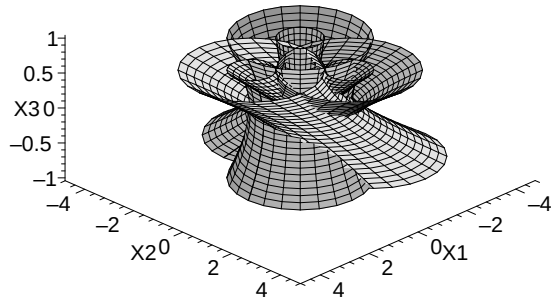

Figure 3: Workspace image of an $R\underline{P}R$-symmetric platform.

where K_1 and K_2 are two circle coordinates, as defined previously, x and y are the coordinates of the platform attachment point expressed in E, r_i is the length of the prismatic joint in the i^{th} leg, t is the tangent of half the orientation angle of the platform, $\tan\varphi/2$, and ζ is an angular parameter arising from the derivation of the parametric equation.

For each leg in the $R\underline{P}R$ platform, the active P-pair has a minimum and a maximum extention. Examining Equation (13) one immediately sees this corresponds to a minimum and a maximum pair of coaxial hyperboloids.

The minimum and maximum constraint hyperboloids for each $R\underline{P}R$ leg must be determined. The image of the reachable workspace of a specific platform reference point is the solid bounded by the six hyperboloids. To obtain the image of the workspace we consider all positions of the reference point for fixed platform orientations for each leg. This involves intersecting the three surface bound solids with the planes X_3 = constant. The corresponding curves are three pairs of concentric circles. The area common to the six circles, if any, is the image of the reachable workspace of the reference point for the specific orientation.

It is a simple matter to determine the pre-image, giving the Cartesian workspace for the reference point. This is done by selecting a reference point, $(x : y : 1)$, then substituting the expressions for the three sets of hyperboloid circles into Equation (7). Again, the area common the the six pre-image curves, if any, is the Cartesian reachable workspace of the reference point for the given platform orientation. The entire Cartesian reachable workspace is the union of all orientation layers. An example of the workspace image is illustrated in Figure 3, while a detailed example is given in [6].

It is easy to see computing the image for another reference point is not difficult. Note, the platform reference point is completely arbitrary: the pre-image depends on the choice for the platform reference point. Examples for the $RR\underline{G}$ and the $P\underline{P}R$ symmetric platforms follow in the next sections.

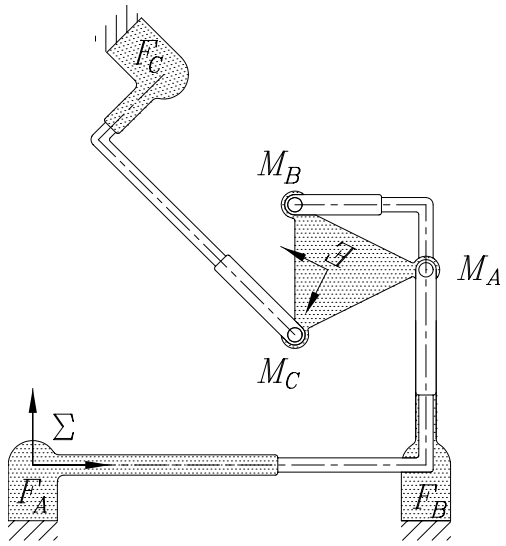

Figure 4: A $P\underline{P}R$-symmetric platform.

5.2 *P<u>P</u>R*-Symmetric Platforms

For each leg in the $P\underline{P}R$ platform the active P-pair has a minimum and a maximum extension. The only variable quantities are the length of the P-pair, and the platform reference point coordinates, $(x : y : z)$; all other quantities are design constants. Hence, for a selected platform reference point there is a minimum and a maximum hyperbolic paraboloid constraint surface corresponding to the minimum and maximum length of the P-pair. It turns out that every pair of hyperbolic paraboloids in a given family have the same curve of intersection because terms dependent on the length of the P-pair can be factored out. This can be seen when the intersection curve is projected into the planes $X_1 = 0$, $X_2 = 0$, $X_3 = 0$ and $X_4 = 0$. Therefore, the whole set of hyperbolic paraboloids in a family forms a pencil of quadrics. The solid bounded by the minimum and maximum hyperbolic paraboloid in each leg is the kinematic image of the platform workspace when the other two legs are disconnected.

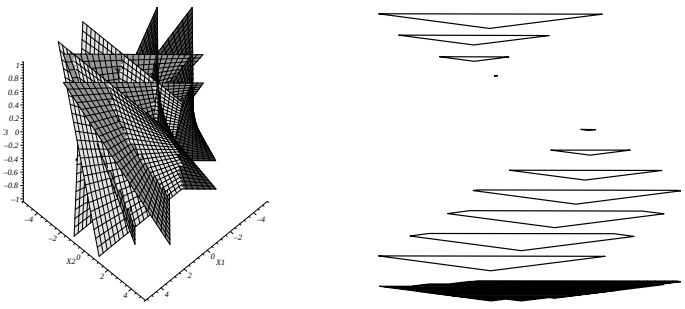

Figure 5: Workspace image; 3D view of workspace layers of a $P\underline{P}R$-symmetric platform.

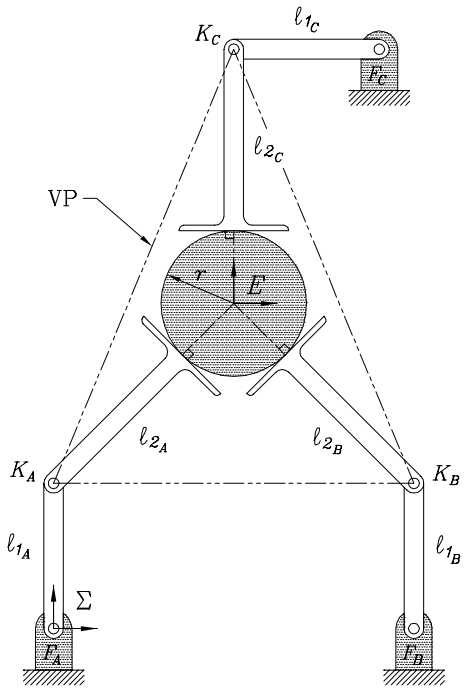

Figure 6: An $RR\underline{G}$-symmetric platform.

The left-hand side of Figure 5 shows the minimum and a maximum hyperbolic paraboloid constraint surfaces corresponding to the minimum and maximum length of the active P-pair in each of the symmetric $P\underline{P}R$ platform legs. Exploiting some geometric properties of the constraint manifold, we can derive the following parametric form [9]:

$$\begin{bmatrix} X_1 \\ X_2 \\ X_3 \end{bmatrix} = \begin{bmatrix} f(t)+s \\ g(t,s) \\ t \end{bmatrix}, \quad \begin{matrix} -\infty \le t \le \infty, \\ -\infty \le s \le \infty, \end{matrix} \tag{14}$$

where t and s are linear parameters and

$$f(t) = \frac{(K_3+2K_1x+2K_2y)t^2+(K_1y-K_2x)4t-2(K_1x+K_2y)+K_3}{4(K_1t-K_2)},$$
$$g(t,s) = \frac{(K_2-K_1t)s}{K_1+K_2t}.$$

The right-hand side of Figure 5 shows different layers of the reachable Cartesian reachable workspace. There are 13 layers, each representing a 30° increment in φ. The top layer represents a platform orientation of 180°, the second from the bottom is that of -180°, while the shaded bottom layer is the union of all the layers. The platform has orientation singularities between approximately 10° and 70°, hence the layers representing 30° and 60° are empty.

5.3 *RR<u>G</u>*-Symmetric Platforms

Perhaps the most interesting, from a geometric perspective, is a three-legged platform possessing an active higher-pair as the

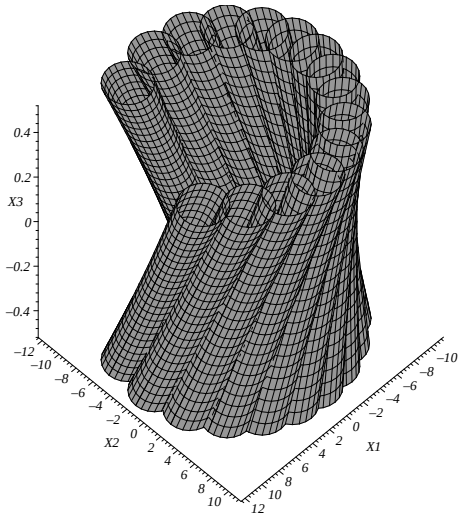

Figure 7: Workspace image of one leg of an $RR\underline{G}$-symmetric platform.

third joint in each kinematic chain. For this type of platform it can be shown, see [16, 11], that the workspace image for each leg consists of the solid bounded by an envelope of hyperboloids of one sheet possessing identical shape parameters, but unique axis. For every value of the higher pair input there corresponds an hyperboloid axis, all belonging to a ruled surface. The solid bounded by the envelope of these hyperboloids is the image of the workspace for that leg when the other two have been disconnected from the pinion. The image of the workspace of the entire platform is the solid region bounded by the intersection of these three envelopes. For the example found in [11], the reachable workspace image of one leg is shown in Figure 7.

The left-hand side of Figure 8 shows different layers of the reachable Cartesian workspace for the reference point taken to be the centre of the pinion. There are 13 layers, each representing a 30° increment in the orientation of the pinion. In right-hand side of Figure 8, the different layers are given different elevations according to the pinion orientation. The top layer is the reachable workspace for a pinion orientation of 180° while the second layer from the bottom is that of -180° orientation. The bottom is the union of all the layers.

The dextrous workspace of a manipulator is usually defined as the set of all points within the reachable workspace that the end-effector can reach with any orientation. Examining the left-hand side of Figure 8, the boundary of the dextrous workspace is seen to be the shaded region that is common to all layers. An area computation reveals that the dextrous workspace comprises 31.71% of the reachable workspace. Moreover, the reachable and dextrous workspace contain no holes; a remarkable result when compared with lower pair jointed three-legged platforms, see [2, 17], or [6], for example.

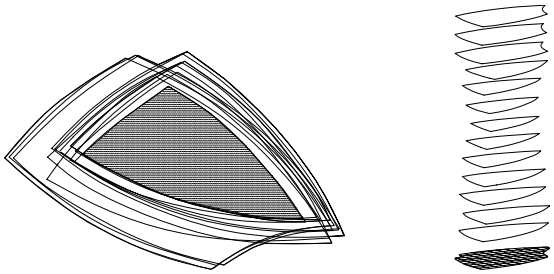

Figure 8: Overlay of workspace layers; 3D view of workspace layers.

5.4 RPR Platform: Different Active Joint in Each Leg

The general case of a three-legged platform can be demonstrated using a platform possessing three RPR legs where the active joint is different in each of the three legs: leg A is RR-type, leg B is PR-type, leg C is RP-type. This platform is illustrated in Figure 9.

5.4.1 FK Example

Here we use the general FK procedure [10] to solve the FK problem of a platform with one each of $\underline{R}PR$, $R\underline{P}R$, and $RP\underline{R}$ legs, shown in Figure 9. The relevant kinematic mapping parameters, listed in Table 2, are the fixed base points $(X : Y : Z)$ expressed in Σ, the relatively moving platform points $(x : y : z)$ expressed in E, the variable joint inputs (the subscripts on β and γ indicate the frame in which the angle is measured counter-clock-wise relative to the X or x axis, respectively), and the corresponding circle coordinates for the platform illustrated in Figure 9.

i	$(X : Y : Z)$	$(x : y : z)$	Input
A	$(0 : 0 : 1)$	$(0 : 0 : 1)$	$d = 2.5$
B	$(6 : 0 : 1)$	$(2 : 0 : 1)$	$\beta_\Sigma = 135^\circ$
C	$(3 : 6 : 1)$	$(1 : 2 : 1)$	$\gamma_E = 45^\circ$

i	$(K_0 : K_1 : K_2 : K_3)$
A	$(1 : 0 : 0 : -4)$
B	$(0 : -\sqrt{2}/4 : -\sqrt{2}/4 : 3\sqrt{2})$
C	$(0 : -\sqrt{2}/4 : -\sqrt{2}/4 : -\sqrt{2}/2)$

Table 2: Kinematic mapping parameters.

The corresponding three constraint surfaces are a hyperboloid of one sheet for the $\underline{R}PR$ leg A, a hyperbolic paraboloid for the $R\underline{P}R$ leg B, and an inversion hyperbolic paraboloid for the $RP\underline{R}$ leg C. The univariate in X_3 (see Eq. 15) is computed together with corresponding values of X_1 and X_2 for the real roots of the univariate, which in this case is 5^{th} order:

$$45X_3^5 - 77X_3^4 + 56X_3^3 + 120X_3^2 - 53X_3 + 5. \qquad (15)$$

The solutions must be carefully inspected. There are three real and one pair of complex conjugate roots. One root, $X_3 =$

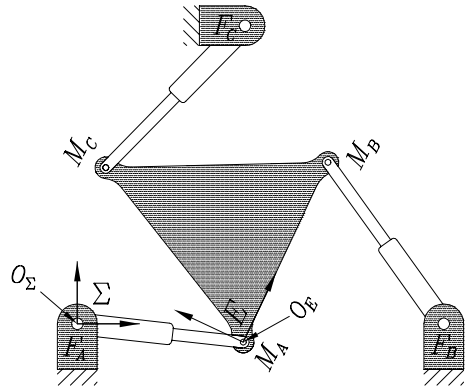

Figure 9: A platform with one each of *RPR, RPR, and RPR* legs.

-1, represents a line that is a common generator between the two hyperbolic paraboloids, but that does not intersect the hyperboloid in any finite points.

The two real roots that lead to solutions are listed in Table 3. The kinematic mapping image of the two solutions can be seen as the two points common to the three surfaces in Figure 10, while the corresponding configurations are illustrated in Figure 11. Note that the common line bewteen the two hyperbolic paraboloids is visible in the same figure.

Solution	a	b	φ (deg)
1	2.2993	0.9814	29.0303
2	1.5837	1.9344	16.3404

Table 3: The two real Cartesian solutions.

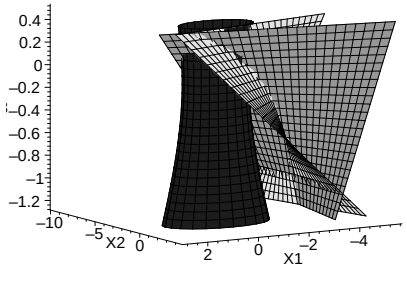

Figure 10: The image of the two real FK solutions.

5.4.2 Workspace

The strategy for determining the kinematic image of the reachable workspace for arbitrary mixed-leg platforms is an extension of the approach to solving the FK. For each leg we determine the constraint surfaces corresponding to the minimum and maximum variable joint inputs. For RR-type legs, the constraint surfaces are hyperboloids of one sheet all sharing the same axis. For RP- and PR-type legs the constraint surfaces are hyperbolic paraboloids, however, the relationship between the minimum and maximum surfaces depends on the type of active joint in the kinematic chain.

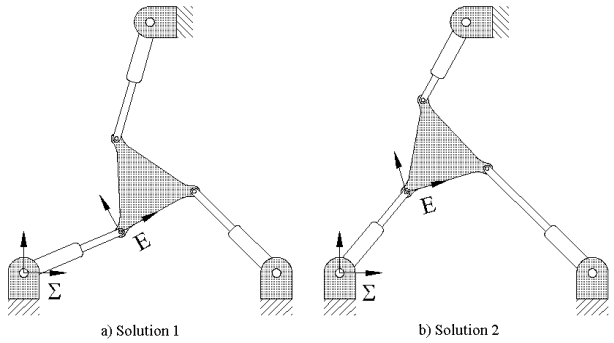

Figure 11: The two real FK solutions.

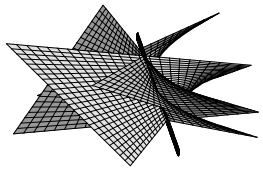

Figure 12: Three hyperbolic paraboloid for three input angles in an *RPR* leg, and *axis*.

When the active joint is an R-pair, pairs of hyperbolic paraboloids in a family still intersect in the same type of degenerate quadratic: a real and imaginary line pair. Figure 12 illustrates three hyperbolic paraboloid constraint surfaces for an RPR leg for three distinct input angles. They all share the line shown in the figure, in a sense the *axis* of the family of hyperbolic paraboloids. The working conjecture is that the the real image space line is finite. Figure 13 shows the hyperboloid family for leg A and the lines of intersection of the hyperbolic paraboloid families belonging to legs B and C.

Summarizing the discussion in Section 5.2, if the active joint is a P-pair, its reach is limited by its minimum and maximum extention. Hence, for a selected platform reference point there is a minimum and a maximum hyperbolic paraboloid constraint surface corresponding to the minimum and maximum length of

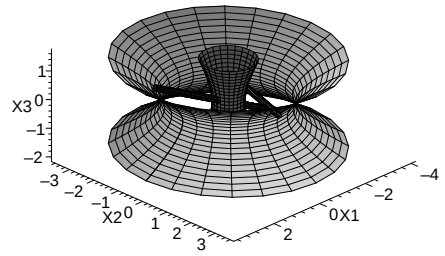

Figure 13: The concentric hyperboloids for leg A and hyperbolic paraboloid axes for legs B and C.

the active P-pair. Every pair of hyperbolic paraboloids in a given family have the same curve of intersection, which degenerates to a real and imaginary line pair. Therefore, the whole set of hyperbolic paraboloids in a family forms a pencil of quadrics. The current working conjecture is that the real line is on the plane at infinity, thus no two hyperbolic paraboloids in one family have finite image points in common, recall the left-hand side of Figure 5. The solid bounded by the minimum and maximum hyperbolic paraboloid in each leg is the kinematic image of the platform workspace when the other two legs are disconnected.

The Cartesian reachable workspace, not shown here, is the pre-image obtained by substituting X_1, X_2, X_3 from either parametric Equations (13), or (14) into either Equations (5), or (6), depending upon the nature of the constraint. The general rules are as follows:

1. RR-type: substitute X_1, X_2, X_3 from Equation (13) into Equation (5).

2. PR-type: substitute X_1, X_2, X_3 from Equation (14) into Equation (5).

3. RP-type: substitute X_1, X_2, X_3 from Equation (14) into Equation (6), being careful to define the coefficients as described in the discussionin Section 4.

6 Conclusions and Future Work

A unified method for determining the reachable workspace of GP3LP, including a sub-class of three-legged platforms with actuated holonomic higher pairs, has been presented. The current state of the determination allows for only the joint limits on the active pairs. In order to be a truly useful tool for designers the passive joint limits must be included in the constraint equations. We are now working with some formulations that could provide this crucial missing component. PP-type leg constraints must also be formulated so as to complete the generalization.

References

[1] J-P. Merlet. Parallel Manipulators: State of the Art and Perspectives. http://www-sop.inria.fr/saga/personnel/merlet/merlet.html, Inst. Nat. de Rech. en Inf. et en Auto, France, 1999.

[2] J. Sefrioui and C.M. Gosselin. "Singularity Analysis and Representation of Planar Parallel Manipulators". *Robotics and Autonomous Systems*, vol. 10: pages 209–224, 1992.

[3] C.L. Collins and J.M. McCarthy. "The Quartic Singularity Surface of Planar Platforms in the Clifford Algebra of the Projective Plane". *Mech. Mach. Theory*, vol. 33, no. 7: pages 931–944, 1998.

[4] C. Gosselin. *Kinematic Analysis, Optimization and Programming of Parallel Robotic Manipulators*. PhD thesis, Dept. of Mech. Eng., McGill University, Montréal, Qc., Canada, 1988.

[5] J-P. Merlet. *Les Robots Parallèles*. Hermès Publishers, Paris, France, 1990.

[6] M.L. Husty. "On the Workspace of Planar Three-legged Platforms". *Proc. World Automation Conf., 6th Int. Symposium on Rob. and Manuf.* (ISRAM 1996), Montpellier, France, vol. 3: pages 339–344, 1996.

[7] J-P. Merlet. "Direct Kinematics of Planar Parallel Manipulators". *IEEE Int. Conf. on Robotics and Automation*, Minneapolis, U.S.A., pages 3744–3749, 1996.

[8] M.J.D. Hayes, M.L. Husty, and P.J. Zsombor-Murray. "Kinematic Mapping of Planar Stewart-Gough Platforms". *Proc. 17th Canadian Congress of Applied Mechanics (CANCAM 1999)*, Hamilton, On., Canada, pages 319–320, 1999.

[9] M.J.D. Hayes and M.L. Husty. "On the Kinematic Constraint Surfaces of General Three-Legged Planar Robot Platforms". Accepted for publication April 2002 in *Mechanism and Machine Theory*, 2002.

[10] P.J. Zsombor-Murrary, C. Chen, and M.J.D. Hayes. "Direct Kinematic Mapping for General Planar Parallel Manipulators". *Proc. CSME Forum 2002*, Kingston, On., Canada, May 21-24, 2002.

[11] M.J.D. Hayes and M.L. Husty. "Workspace Characterization of Planar Three-legged Platforms With Holonomic Higher Pairs". *Advances in Robotic Kinematics*, eds. Lenarčič, J., Stanišić, Kluwer Academic Publishers, Dordrecht, The Netherlands, pages 267–276, 2000.

[12] M.J.D. Hayes. *Kinematics of General Planar Stewart-Gough Platforms*. PhD thesis, Dept. of Mech. Eng., McGill University, Montréal, Qc., Canada, 1999.

[13] W. Blaschke. “Euklidische Kinematik und Nichteuklidische Geometrie”. *Zeitschr. Math. Phys.*, vol. 60: pages 61–91 and 203–204, 1911.

[14] J. Grünwald. “Ein Abbildungsprinzip, welches die ebene Geometrie und Kinematik mit der räumlichen Geometrie verknüpft”. *Sitzber. Ak. Wiss. Wien*, vol. 120: pages 677–741, 1911.

[15] O. Bottema and B. Roth. *Theoretical Kinematics*. Dover Publications, Inc., New York, N.Y., U.S.A., 1990.

[16] M.J.D. Hayes, M.L. Husty, and P.J. Zsombor-Murray. “Solving the Forward Kinematics of a Planar 3-legged Platform With Holonomic Higher Pairs”. *ASME, Journal of Mechanical Design*, vol. 121, no. 2: pages 212–219, 1999.

[17] J. Sefrioui and C.M. Gosselin. “On the Quadric Nature of the Singularity Curves of Planar Three-Degree-of-Freedom Parallel Manipulators”. *Mech. Mach. Theory*, vol. 30, no. 4: pages 533–551, 1995.

[18] M.J.D. Hayes, M.L. Husty, and P.J. Zsombor-Murray. “Towards Workspace Analysis of Platforms with Three Arbitrary Legs”. *Proc. 18th Canadian Congress of Applied Mechanics (CANCAM)*, St. John’s NF. Canada, pages 355–356, 2001.